The Response of Ocean Waves to Turning Winds

WILLIAM PERRIE AND BECHARA TOULANY

Physical and Chemical Sciences, Scotia-Fundy Region, Department of Fisheries and Oceans, Bedford Institute of Oceanography, Dartmouth, Nova Scotia, Canada

(Manuscript received 14 December 1993, in final form 13 September 1994)

ABSTRACT

A model is developed for the response of waves to turning wind, which we denote as the *fetch* relaxation model. Comparison is presented with the standard δ relaxation model pioneered by Hasselmann et al. The *fetch* relaxation model is shown to surpass the standard δ model, with respect to observations collected during the Canadian Atlantic Storm Program (CASP) of 1986. Both models are based on the premise that the net growth of energy due to the wind is centered on the wind direction. The *fetch* relaxation model also conforms to relations for fetch-limited growing waves derived from the CASP observations. Moreover, the *fetch* relaxation model is shown to provide estimates for the role of the drag coefficient in turning wind situations.

1. Introduction

Despite recent efforts by Van Vledder and Holthuijsen (1993), Masson (1990), Holthuijsen et al. (1987), Young et al. (1987), Allender et al. (1983), and Hasselmann et al. (1980), the response of ocean waves to forcing by wind fields with a varying wind direction is inadequately understood. This is the result of the difficulty both in collecting good observations and also in the formulation of a cogent model for all the relevant dynamical processes. In contrast, the fetch-limited response of waves to constant offshore winds is fairly well understood, as shown by the JONSWAP experiment of Hasselmann et al. (1973), the Lake Ontario data of Donelan et al. (1985), and many other research efforts. In this paper, we therefore introduce a new model for the response of waves to turning wind directions, motivated by the success of fetch-limited relations for growing waves. Verification of the model is found in the directional wave buoy observations of Dobson et al. (1989) collected during the Canadian Atlantic Storm Program (CASP) of 1986.

The analysis of directional buoy data by Holthuijsen et al. (1987) is representative of the standard approach, used in many studies, for understanding the response of waves to turning winds. Holthuijsen et al. (1987) used a relaxation model of the form

$$\frac{\partial \theta_0}{\partial t} = \frac{1}{\tau} \sin(\theta_{10} - \theta_0), \qquad (1.1)$$

where θ_{10} is the wind direction and τ is a measure of the response time for the mean wave direction θ_0, defined as

$$\theta_0 = \arctan\left\{\frac{\int_0^{2\pi}\int_0^{\infty} E(f,\theta)\sin\theta\, df d\theta}{\int_0^{2\pi}\int_0^{\infty} E(f,\theta)\cos\theta\, df d\theta}\right\}, \qquad (1.2)$$

and where $E(f,\theta)$ is the spectral wave energy as a function of frequency f and wave direction θ. Analysis of observed data, using models similar to Eq. (1.1), led to the concept that the response of the overall wave field depends on spectral wave maturity parameters such as inverse wave age. This was supported by Günther et al. (1981), Holthuijsen et al. (1987), Masson (1990), and Van Vledder and Holthuijsen (1993). Recently Gao and Komen (1993) extended the approach of Holthuijsen et al. (1987). Following Holthuijsen et al. (1987), they derived a generalization of Eq. (1.1) using the energy balance equation

$$\frac{\partial E(f,\theta:\mathbf{x},t)}{\partial t} + \nabla \cdot C_g E(f,\theta:\mathbf{x},t) = S, \qquad (1.3)$$

where $E(f,\theta:\mathbf{x},t)$ is the two-dimensional wave spectrum, f is the frequency, θ is direction, $\mathbf{x}$ is position, and t is time. In place of θ_{10} in Eq. (1.1), they introduced $\theta_{\partial E/\partial t}$, defined as

$$\theta_{\partial E/\partial t} = \arctan\left\{\frac{\int_0^{2\pi}\int_0^{\infty} \sin\theta \frac{\partial}{\partial t} E(f,\theta) df d\theta}{\int_0^{2\pi}\int_0^{\infty} \cos\theta \frac{\partial}{\partial t} E(f,\theta) df d\theta}\right\}, \qquad (1.4)$$

Corresponding author address: Dr. William Perrie, Bedford Institute of Oceanography, P.O. Box 1006, Dartmouth, NS B2Y 4A2, Canada.
Email: wperrie@emerald.bio.ns.ca

where the relaxation time is expressed as

$$\tau = \frac{\cos\theta_{\partial E/\partial t} \int_0^{2\pi} \int_0^{\infty} E(f, \theta) \cos\theta df d\theta}{\cos\theta_0 \int_0^{2\pi} \int_0^{\infty} \cos\theta \frac{\partial}{\partial t} E(f, \theta) df d\theta}. \quad (1.5)$$

Alternately, using the cospectra and quadspectra notation of Longuet-Higgins et al. (1963), $\mathcal{L}_1 \equiv \int_0^{2\pi} \sin\theta E(f, \theta) d\theta$ and $a_1 \equiv \int_0^{2\pi} \cos\theta E(f, \theta) d\theta$, the expression for $\theta_{\partial E/\partial t}$ may be rewritten as

$$\theta_{\partial E/\partial t} = \arctan\left\{ \frac{\partial \bar{\mathcal{L}}_1}{\partial t} \Big/ \frac{\partial \bar{a}_1}{\partial t} \right\}, \quad (1.6)$$

where the overbar denotes average over the whole frequency domain. Gao and Komen (1993) demonstrated an enhanced comparison with data, compared to the approach of Holthuijsen et al. (1987). Moreover, they found that θ_{10} differs from $\theta_{\partial E/\partial t}$, which is to be expected from the form of Eq. (1.6).

A frequency-dependent generalization of Eq. (1.1) constitutes the standard $\mathcal{L}$ relaxation models pioneered by Hasselmann et al. (1980):

$$\frac{\partial \bar{\theta}(f)}{\partial t} = \mathcal{L}\omega \sin[\theta_{10} - \bar{\theta}(f)], \quad (1.7)$$

where $\bar{\theta}(f)$ is the mean wave direction at wave frequency f determined from the cospectra and quadspectra as discussed in section 2, $\mathcal{L}$ is a relaxation function to be determined empirically, θ_{10} is the direction of the reference wind speed $\mathcal{U}$ at time t, and ω is the angular frequency $2\pi f$. Effectively $\mathcal{L}\omega$ is an inverse timescale, which may be expressed as $1/\tau$, for the response of the waves at frequency f to turning winds. From the analysis of observations, Hasselmann et al. (1980), Günther et al. (1981), Allender et al. (1983), and Masson (1990) found that τ varies inversely with frequency f. Numerical confirmation that τ could decrease with increasing f was provided by Young et al. (1987) using the EXACT-NL model of Hasselmann and Hasselmann (1985) to explicitly represent wave generation, nonlinear wave–wave interactions, and wave dissipation. Van Vledder and Holthuijsen (1993) extended the numerical simulations of Young et al. (1987) and did a detailed study of the role of the relevant physical processes. They also performed a reanalysis of old results in an attempt to explain the wide variation reported in earlier analyses for the relaxation constants. Moreover, they reported differences between observed timescales and computed timescales, which may result from inadequacies in the model. For example, the drag coefficient may be higher for waves off the main direction of the spectrum. Therefore, in spectral wave directions off the main wind direction, young waves may develop that are rougher than old waves. Although this has impact on parameterizations for the input of energy into waves, it was not considered by the EXACT-NL model they used.

A new model for the response of waves to turning winds can be motivated from the fact that in the analysis of observed fetch-limited growing spectra from JONSWAP or CASP, for example, turning wind episodes are frequently embedded within sets of observations that are largely regarded as fetch-limited growing spectral cases. That is, turning wind episodes often occur in situations where the wind direction is explicitly offshore throughout the entire turning wind (fetch limited) event. Resultant fetch-limited relations derived both by Perrie and Toulany (1990) for CASP and by Hasselmann et al. (1973) for JONSWAP correlate well with observations. Moreover, the existence of turning wind episodes embedded within fetch-limited growing cases occurs in any experiment involving directional buoys because the selection criteria for fetch-limited episodes is generally that the wind direction be about ±30° from orthogonal to offshore, which is a wide sector.

Section 2 presents an analysis of CASP observations with respect to the standard $\mathcal{L}$ relaxation model of Eq. (1.7). A frequency-dependent relation for $\mathcal{L}$ is derived. Section 3 develops a fetch-limited model for the response of wave spectra to turning winds, hereafter denoted the *fetch* relaxation model. The key element of the *fetch* relaxation model is the fetch-limited wave growth relations established by Perrie and Toulany (1990) based on scaling by $\mathcal{U}_{*c}$, the friction velocity component in the direction of the wave spectrum at the peak frequency f_p. Constraints associated with the *fetch* relaxation model for data selection and analysis are presented in section 4. Verification of the *fetch* relaxation model is given in section 5, and implications for the behavior of the drag coefficient in section 6.

2. $\mathcal{L}$ Relaxation model

To provide a baseline for comparison with the *fetch* relaxation model developed in sections 3–5, we first present the $\mathcal{L}$ relaxation model, following Hasselmann et al. (1980), Masson (1990), and Van Vledder and Holthuijsen (1993). This model is described by Eq. (1.7). The mean wave direction at frequency f, denoted $\bar{\theta}(f)$, is defined for a directional buoy from the quadspectra between the heave signal and the north–south wave slope Q_{12}, and the heave signal and the east–west slope Q_{13},

$$\bar{\theta}(f) = \arctan\left(-\frac{Q_{13}}{Q_{12}} \right), \quad (2.1)$$

corrected for the magnetic declination. Angles defined by $+\frac{3}{2}\pi \leq \theta(f)$ and $\theta(f) \leq +\pi/2$ were specified as in the domain $-\pi/2 \leq \theta(f) \leq +\pi/2$ to correctly obtain a mean direction by averaging angles varying from $(2\pi)^-$ to 0^+. Equation (2.1) avoids the 180° ambiguity encountered using raw time series data.

Equation (1.7) is generic to the so-called ℓ models in the sense that one could also consider several variations of Eq. (1.7). For example,

$$\frac{\partial\bar{\theta}(f)}{\partial t} = \ell\omega \frac{\mathcal{C}(f)}{\mathcal{U}} \sin[\theta_{10} - \bar{\theta}(f)], \qquad (2.2)$$

where $\mathcal{C}(f)$ is the phase speed, and so forth. In each case, we have found that comparison of the ℓ relaxation model of Eq. (1.7) or (2.2) with CASP measurements gives about the same results. The correlation coefficients are at best in the range 0.5–0.6. In this study we present results only for the model described by Eq. (1.7).

Selection criteria for the wave response to turning wind episodes were essentially the same as those of Masson (1990), Hasselmann et al. (1980), and others. For every studied frequency f (and corresponding wavenumber k):

(i) finite depth effects were avoided by requiring that $kh \geq \pi/2$,

(ii) only observed wind wave $E(f)$ was included for which $E(f) \geq 0.1 \times E(f)_{\text{max wind waves}}$, to avoid noise,

(iii) observations were required to obey $\mathcal{U}/\mathcal{C}(f) \geq 1$ to ensure that the wind speed is high enough to generate wind waves, and as a first-order elimination of swell, and

(iv) observations must have obeyed $\mathcal{U}/\mathcal{C}(f) \leq 2$ to ensure that the wind is not too high and to avoid low frequency wind wave shoaling.

"Noise" is understood to refer to scales of motion or modes of dynamics unrelated to the specific observations with which we are concerned. The subscript "max wind waves" denotes the maximum of the wind wave spectrum in one dimension $E(f)$, excluding swell. Whereas swell constitutes a problem for the *fetch* relaxation model presented in section 3 because swell energy can seriously bias estimates of wave growth energy used to establish fetch relations, swell is not a problem for the ℓ relaxation model. This follows from the fact that the ℓ relaxation model is a function of frequency as specified by the relaxation timescale τ. Because swell components within the spectrum have long timescales, which essentially do not respond to turning winds, and because they occur at low frequencies, they are eliminated by constraints (i) and (iii). This is demonstrated in Table 1c.

Figure 1 shows the array of directional wave buoys deployed off the Nova Scotia coast during the CASP experiment, as presented by Dobson et al. (1989). The buoys were deployed along a line bearing 160°T orthogonal to the coastline in water of depth 22 m, 50 m, and 100 m. The buoys record for 30 minutes hourly with a sampling rate of 0.78125 s. Nyquist frequency f_N is 0.64 Hz. A meteorological buoy (MINIMET) at the seaward end of the wave buoy array recording wind speed and direction is also shown. The meteorological buoy was part of the network of mesoscale meteorological stations along the coast. The height for wind measurements was 3 m at the meteorological buoy and 10 m at the coastline stations. The meteorological buoy winds were converted to 10-m reference heights using the air–sea temperature difference to take account of stable, unstable, and neutral conditions following Smith (1981). Resultant wind data were averaged hourly.

An extensive discussion of the observations recorded by the meteorological buoy and tests for observation accuracy appears in Dobson et al. (1989). Buoy winds were first converted to a 10-m measurement height. The air temperature at the shoreline station on Martinique Beach and the sea temperature at the meteorological buoy were used to allow for atmospheric stability following Smith (1981). Comparison was made with the shoreline wind speeds recorded at the shoreline station. When winds were onshore and stationary (within ±50° of the offshore normal with no hourly changes >20%), buoy winds agreed with Martinique Beach winds to within 1.5% with standard error of 2.5%. Other calibrations were performed with routine meteorological measurements at Shearwater Airport in Dartmouth, Nova Scotia, and laboratory calibrations before and after deployment. Buoy wind sensors were estimated by Dobson et al. (1989) to have an error of ±4% in wind speed and ±2.5° in wind direction.

The directional wave buoys (Datawell WAVEC buoys) recorded the cross spectra between all pairs of raw time series data for heave, north–south slope, and east–west slope. Measurements were averaged half-hourly on each hour. The cospectra and quadspectra were initially computed with a resolution of 0.005 Hz and 18 degrees of freedom from the time series of the vertical acceleration and the north and east components of the slope recorded by the directional wave buoys. Statistically stable estimates were obtained by smoothing. That is, averages were computed on ten adjacent frequency bands to give a resultant resolution of $\Delta f = 0.05$ with 180 degrees of freedom. The 12 resultant frequency bands, centered at 0.0525, 0.1025, 0.1525, . . . , 0.6025 Hz, were used in the analysis. In effect, it was found that the middle four or five of these frequencies, starting at 0.2025 Hz, were most responsive to changing wind directions. All data below 0.03 Hz were quite noisy and were simply left out of the averaging. Resultant wave responses to changing wind directions computed from these cospectra and quadspectra were found to be more stable than results obtained by first computing the wave directions at each frequency band with $\Delta f = 0.005$ Hz and then averaging on groups of neighboring bands.

From the CASP experiment, two episodes of turning winds were considered for analysis by the ℓ relaxation model of this section and the *fetch* relaxation model of the next sections:

(i) 39 hours from 0900 UTC 30 January to 2300 UTC 31 January and

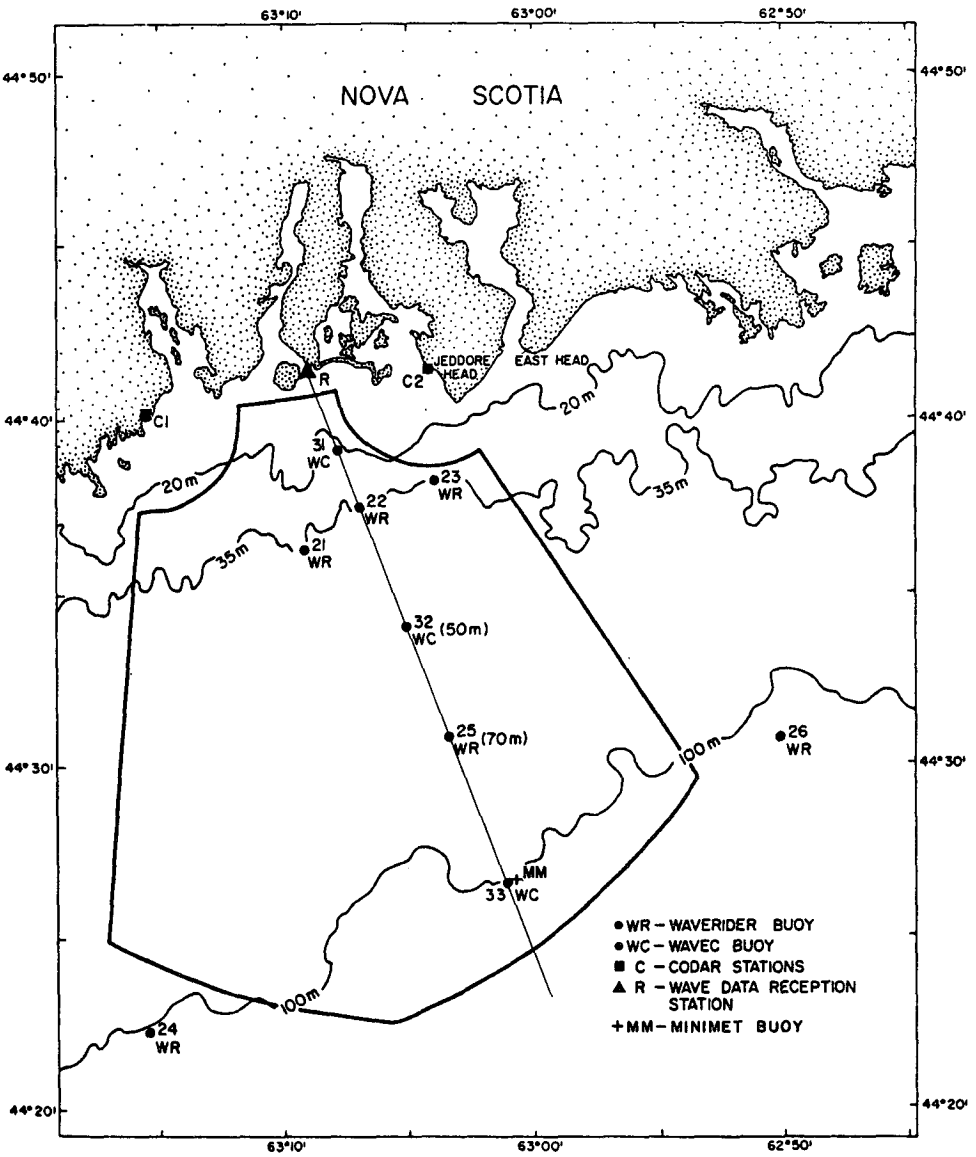

FIG. 1. The CASP wave buoy array. The range of wave and surface current measurements from CODAR radar is indicated (solid line).

(ii) 72 hours from 0000 UTC 14 February to 2300 UTC 16 February.

Except for episode (i), when the outermost wave buoy WC33 did not function, all directional buoys recorded observations reliably during these episodes. Correlation coefficients for the ℓ relaxation model were highest for all of episode (i) and the middle portion of episode (ii), specifically 25 hours from 0000 UTC 15 February to 0000 UTC 16 February. Episode (i) and the 25-h subset of episode (ii) are hereafter denoted OP1 (Observing Period 1) and OP2, respectively.

Ideally, one may like to study the response of waves to turning winds when the wind is constant and turning at a (not too fast) constant prescribed rate. However, this is never the case. The rate of turning of the wind varies with time, as does the wind speed. In Figs. 2a–b, we present the time series of the wind speed and direction and nine frequency bands, obtained by averaging groups of three adjacent frequency bands of the wave spectra, centered at 0.10, 0.16, 0.22, . . . , 0.58 Hz, as observed at the middle buoy WC32 during OP1 and OP2. These frequency bands were chosen simply to display the response of the waves to turning winds. The 12 frequency bands used in the analysis of the ℓ relaxation model are centered at 0.0525, 0.1025, 0.1525, . . . , 0.6025 Hz, as mentioned above. Figures 2a–b show the tendency of the wave spectra to migrate

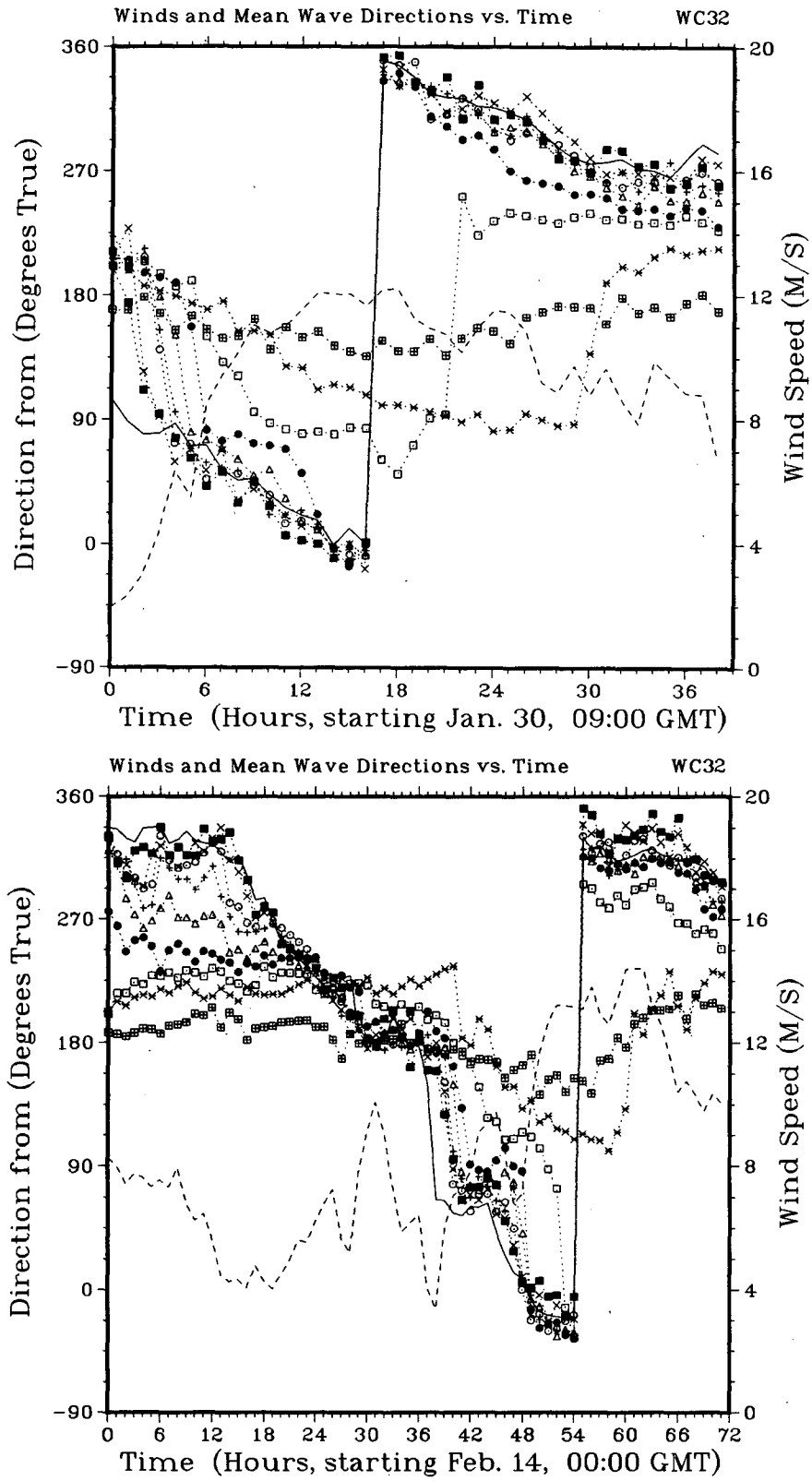

FIG. 2. (a: top) The times series of the wind speed (dashed) and direction (solid) and also the frequency bands: 0.10 (quad-squares), 0.16 (asterisks), 0.22 (open square), 0.28 (solid dots), 0.34 (triangles), 0.40 (crosses), 0.46 (open circles), 0.52 (×'s), and 0.58 (solid squares) of the wave spectra as observed at the center directional buoy WC32 during episode (i). (b: bottom) As in (a) but for episode (ii).

towards the direction of the forcing wind as time evolves. The highest wave spectral frequencies respond most quickly, whereas lower frequencies have a much longer timescale of response. The very lowest frequency, for example 0.10 Hz, did not see the change in wind direction during OP1 or OP2. This is a qualitative verification of the behavior for the relaxation time τ, as presented by Young et al. (1987). Of course, nonuniformities in both the rate of change of wind direction and the wind speed as a function of position and throughout the duration of OP1 and OP2 complicate both τ and the wave responses shown in Figs. 2a–b.

Results of a regression analysis of the data in episodes OP1 and OP2 using the ℓ relaxation model presented in Eq. (1.7) are given in Tables 1a–c. The correlation coefficients $\mathcal{R}$, for OP1 and OP2 taken together, are in the range 0.36–0.67, with an overall correlation of 0.55 on 493 observations. Correlations for OP1 and OP2 considered individually are similar. Masson (1990) considered somewhat different portions of the CASP dataset and reported comparable correlations. Table 1c estimates the errors in the calculations as being in the range 30%–100%. The bulk of the Van Vledder and Holthuijsen (1993) data gave a correlation coefficient $\mathcal{R}$ of 0.31 on 133 observations, whereas Hasselmann et al. (1980) found $0.29 \leqslant \mathcal{R} \leqslant 0.40$.

Masson (1990) reported overall values for $\ell \approx 2.5 \times 10^{-5}$, while Allender et al. (1983) found $\ell \approx 1.7 \times 10^{-5}$ and Hasselmann et al. (1980) found $\ell \approx 3.1 \times 10^{-5}$. As Table 1c and Fig. 3 show, our resultant ℓ follows the variation

$$\ell \approx (11.2f - 0.06) \times 10^{-5} \tag{2.3}$$

with a correlation coefficient of 0.97. Although the maximum value ($\approx 6 \times 10^{-5}$) for ℓ exceeds the values reported by Masson (1990) and others, the mean (3.9×10^{-5}) is comparable. The maximum value ($\approx 6 \times 10^{-5}$) is more or less comparable with the reanalyzed results of Allender et al. (1983) and Hasselmann et al. (1980), as discussed by Van Vledder and Holthuijsen (1993). The trend for ℓ to increase with higher frequencies f also seems clear in the CASP data. However, the variation of ℓ with frequency f in Eq. (2.3) is not as fast as was found from numerical simulations by Young et al. (1987).

3. A fetch-limited model for the wave response to turning winds

During fetch-limited growth, the analysis and nondimensionalization of wave variables, such as total energy E_0, has commonly used the wind speed $\mathcal{U}$ (Hasselmann et al. 1973). Following Janssen et al. (1987) and Kahma and Calkoen (1992), an alternate scaling of E_0 is, in terms of the friction velocity $\mathcal{U}_*$,

$$E_0^* = E_0 g^2 / \mathcal{U}_*^4. \tag{3.1}$$

Extending Eq. (3.1), Perrie and Toulany (1990) introduced the scaling of wave variables by the compo-

TABLE 1. Correlation coefficients $\mathcal{R}$ and $\ell \times 10^4$ for the ℓ relaxation model for OP1, episode OP2, and combined episodes OP1 + OP2. Frequency bands centered at 0.0525, 0.1025, 0.1525, . . . , 0.6025 Hz are listed across the top by the numbers 1, 2, 3, . . . , 12. For any subset of this data, such as frequency band 11 of wave buoy WC32, regression analysis was not done if there were less than seven observations. The composite of all frequencies is denoted all. In (c), at frequency band 1, the constraint (i) $kh \geqslant \pi/2$ is broken all the time and at frequency band 2, wave buoy WC31 always has $kh < \pi/2$ and the other buoys, WC32 and WC33, have $\mathcal{U}/\mathcal{C}(f) < 1$, violating constraint (iii).

	1	2	3	4	5	6	7	8	9	10	11	12	All
						(a) OP1							
Number of observations			18	64	57	32	14	5	5	6	6	4	211
$\mathcal{R}$			.60	.43	.43	.66	.71						.56
$\ell \times 10^4$			.21	.21	.14	.22	.42						.37
Percent error			62	51	51	44	59						19
						(b) OP2							
Number of observations				24	51	63	55	41	28	13	6	0	282
$\mathcal{R}$				.43	.42	.43	.50	.56	.60	.71			.55
$\ell \times 10^4$				.31	.36	.36	.37	.43	.41	.48			.41
Percent error				92	59	51	45	48	50	62			19
						(c) OP1 + OP2							
Number of observations			18	88	108	95	69	46	34	19	12	4	493
$\mathcal{R}$			.60	.50	.36	.45	.52	.56	.57	.67	.49		.55
$\ell \times 10^4$			.21	.23	.22	.30	.39	.47	.46	.59	.62		.39
Percent error			62	31	41	35	45	49	57	54	108		19

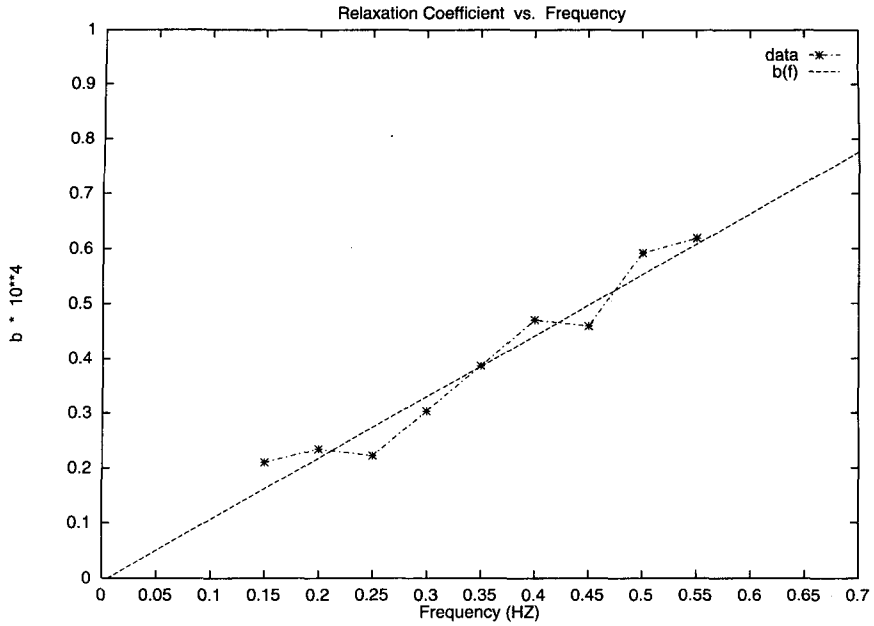

FIG. 3. The variation of ℓ as a function of frequency f.

nent friction velocity $\mathcal{U}_{*c}$ in the direction of the spectral peak frequency f_p, where $\mathcal{U}_*$ is related to $\mathcal{U}_{*c}$ through the relation

$$\mathcal{U}_{*c} \equiv \mathcal{U}_* \cos[\Delta\theta(f_p)], \tag{3.2}$$

and where $\Delta\theta(f_p)$ is the mean wave direction at the spectral peak $\bar{\theta}(f_p)$ minus the 10-m wind direction θ_{10}. Friction velocity $\mathcal{U}_*$ is related to wind speed $\mathcal{U}$ at a given reference height such as 10 m, by the drag coefficient C_d,

$$\mathcal{U}_* \equiv \mathcal{U}\sqrt{C_d}. \tag{3.3}$$

The motivation for the introduction of $\mathcal{U}_{*c}$ in Perrie and Toulany (1990) is given by Donelan et al. (1985), who noted that waves are not the result of strictly local generation but instead are the cumulative result of an evolution along their entire fetch. If the gradient of fetch about the wind direction is large, the wave direction is therefore biased toward long fetch where a lower generating force is more than compensated by the longer fetch over which it operates. Consequently, $\mathcal{U}_{*c}$ contains the directions of both the wind θ_{10} and the mean wave direction at the spectral peak $\bar{\theta}(f_p)$, which we also denote θ_p.

Three possibilities may be considered for the drag coefficient: C_{d1} a constant, C_{d2} the long fetch open-ocean parameterization found by Smith (1988), and C_{d3} a wave age–dependent drag coefficient motivated by Donelan (1982). The constant drag coefficient C_{d1} may be defined as

$$C_{d1} = 1.3 \times 10^{-3}. \tag{3.4}$$

Smith (1988) used a stable tower at the mouth of Halifax Harbour to measure the drag coefficient for open-ocean long fetch conditions and found a dependence on $\mathcal{U}$ and ΔT, the difference between air and water temperatures. This drag coefficient C_{d2} may be represented as

$$C_{d2} = C_d[\mathcal{U}, \Delta T]. \tag{3.5}$$

In the recent Humidity Experiment over the Sea (HEXOS), Smith et al. (1992) measured the drag coefficient for young generating waves and related it to wave age $\mathcal{C}_p/\mathcal{U}_c$ expressed in terms of $\mathcal{U}_c$, the component wind velocity in the direction of the waves at f_p, and $\mathcal{C}_p$ the phase velocity at f_p. Denoted C_{d3}, this drag coefficient was given the approximation

$$C_{d3} = \begin{cases} C_{d2} + (1.51 - 1.87\mathcal{C}_p/\mathcal{U}_c) \times 10^{-3}, \\ \qquad\qquad 0 < \mathcal{C}_p/\mathcal{U}_c < 0.81 \\ C_{d2}, \quad \text{otherwise} \end{cases} \tag{3.6}$$

by Perrie and Toulany (1990). We emphasize that minor corrections are provided to this formulation by the HEXOS data of Smith et al. (1992). However, as analysis of the HEXOS data did not use observations involving the presence of either swell or turning winds, neither C_{d3} nor the formulation of Smith et al. (1992) is completely adequate for turning winds. In any case, with respect to CASP observations Perrie and Toulany (1990) considered scaling with C_{d1}, C_{d2}, and C_{d3} and showed that scaling with $\mathcal{U}_{*c}$ and C_{d3} resulted in the most consistent set of fetch relations.

Following Perrie and Toulany (1990) and Eqs. (3.1)–(3.2), dimensionless wave variables, such as total energy E_0^{*c},

$$E_0^{*c} \equiv E_0 g^2/\mathcal{U}_{*c}^4 \tag{3.7}$$

can be parameterized by a simple fetch-law relation involving dimensionless fetch X^{*c} specified as

$$E_0^{*c} = \mathcal{E}(X^{*c})^e, \tag{3.8}$$

or alternately in terms of inverse wave age $\mathcal{U}_{*c}/\mathcal{C}_p$,

$$E_0^{*c} = \mathbf{E}(\mathcal{U}_{*c}/\mathcal{C}_p)^\gamma, \tag{3.9}$$

where dimensionless fetch X^{*c} is defined as

$$X^{*c} \equiv Xg/\mathcal{U}_{*c}^2, \tag{3.10}$$

where g is the acceleration due to gravity, and e, $\mathcal{E}$, and $\mathbf{E}$ are appropriate constants. Equation (3.9) is particularly important because it is a fetch relation involving only total energy E_0^{*c} and inverse wave age $\mathcal{U}_{*c}/\mathcal{C}_p$, which are open-ocean variables specifying spectral maturity. It should be noted that fetch relations in terms of inverse wave age, such as Eq. (3.9), obtained correlation coefficients consistently as high as 0.99 with respect to the CASP dataset. By comparison, relations in terms of dimensionless fetch X^{*c}, as in Eq. (3.8), obtained correlation coefficients of only 0.92.

Substituting Eqs. (3.2), (3.3), and (3.7) into Eq. (3.9), the corresponding dimensional relation is

$$E_0 = \mathbf{C}_0 \mathcal{U}^{4+\gamma}(\cos^{4+\gamma}\Delta\theta(f_p))C_d^{(4+\gamma)/2} f_p^{\gamma}, \tag{3.11}$$

where $\mathbf{C}_0$ and γ are appropriate constants reported in Perrie and Toulany (1990). Equation (3.11) may be differentiated with respect to time t to imply

$$\frac{\partial\theta_p}{\partial t} = \frac{\partial\theta_{10}}{\partial t} - \frac{1}{\tan\Delta\theta(f_p)}\left(\frac{1}{E_0(4+\gamma)}\frac{\partial E_0}{\partial t} - \frac{\gamma}{f_p(4+\gamma)}\frac{\partial f_p}{\partial t} - \frac{1}{\mathcal{U}}\frac{\partial \mathcal{U}}{\partial t} - \frac{1}{2C_d}\frac{\partial C_d}{\partial t}\right), \tag{3.12}$$

or alternately

$$\frac{\partial\theta_p}{\partial\theta_{10}} = 1 - \frac{1}{\tan\Delta\theta(f_p)}\left(\frac{1}{E_0(4+\gamma)}\frac{\partial E_0}{\partial\theta_{10}} - \frac{\gamma}{f_p(4+\gamma)}\frac{\partial f_p}{\partial\theta_{10}} - \frac{1}{\mathcal{U}}\frac{\partial \mathcal{U}}{\partial\theta_{10}} - \frac{1}{2C_d}\frac{\partial C_d}{\partial\theta_{10}}\right) \tag{3.13}$$

after some algebraic operations. Equation (3.12) is important because it predicts the turning rate, given other measurable quantities. Because time is the implicit independent variable of Eq. (3.13), it is understood that for any variable X of this equation,

$$\partial X \equiv X(t+1) - X(t), \tag{3.14}$$

and we effectively use the mean value $\bar{X}$ between two consecutive time steps,

$$\frac{\partial\theta_p}{\partial\theta_{10}} = 1 - \overline{\tan^{-1}\Delta\theta(f_p)}\left(\frac{1}{\overline{E_0}(4+\gamma)}\frac{\partial E_0}{\partial\theta_{10}} - \frac{\gamma}{\overline{f_p}(4+\gamma)}\frac{\partial f_p}{\partial\theta_{10}} - \frac{1}{\overline{\mathcal{U}}}\frac{\partial \mathcal{U}}{\partial\theta_{10}} - \frac{1}{2\overline{C_d}}\frac{\partial C_d}{\partial\theta_{10}}\right), \tag{3.15}$$

where

$$\bar{X} = \tfrac{1}{2}[X(t+1) + X(t)]. \tag{3.16}$$

We hereafter neglect the overbars in Eq. (3.15). Equation (3.15) is a general relation for the change of wave direction at the spectral peak $\theta_p \equiv \bar{\theta}(f_p)$, given an incremental change in the wind direction $\Delta\theta_{10}$.

The *fetch* model represented by Eq. (3.12) is clearly different from the $\mathcal{L}$ relaxation model discussed in section 2. In its derivation, Eq. (3.12) is related to the fetch relations (3.8)–(3.9), whereas, as presented by Holtjuisen et al. (1987), the $\mathcal{L}$ relaxation model is related to the spectral balance equation (1.3). Equation (3.12) concerns the response of the spectral peak, whereas the $\mathcal{L}$ relaxation model of Eq. (1.7) gives directional relaxation as a function of spectral frequency. Clearly, the spectral relaxation estimates $\partial\bar{\theta}(f)/\partial t$ given by the $\mathcal{L}$ model cannot be derived from the *fetch* model. However, knowing the position of the spectral peak f_p in the observations used in the $\mathcal{L}$ model allows estimation of $\partial\overline{\theta(f_p)}/\partial t$ from Eq. (1.7), which may be compared with corresponding values from the *fetch* model (3.12). In terms of degrees of freedom, Eq. (3.12) depends on six independent variables: θ_{10}, C_d, E_0, γ, f_p, and $\mathcal{U}$; whereas the $\mathcal{L}$ relaxation model (1.7) depends only on two variables: θ_{10} and $\mathcal{L}$. Moreover, the generalized relaxation model (1.1) of Holthuijsen et al. (1987) and Gao and Komen (1993) can also be written in terms of two variables:

$$\frac{\partial\theta_0}{\partial t} = \frac{1}{\tau}\sin\left\{\arctan\left\{\frac{\partial\bar{\mathcal{L}}_1}{\partial t}\Big/\frac{\partial\bar{a}_1}{\partial t}\right\} - \theta_0\right\}, \tag{3.17}$$

where

$$\tau = \frac{\bar{a}_1\cos\left\{\arctan\left\{\dfrac{\partial\bar{\mathcal{L}}_1}{\partial t}\Big/\dfrac{\partial\bar{a}_1}{\partial t}\right\}\right\}}{\left\{\dfrac{\partial}{\partial t}\bar{a}_1\right\}\cos\theta_0}. \tag{3.18}$$

The overbar denotes the average over the frequency domain. Therefore, the *fetch* model of Eq. (3.12) has more degrees of freedom than the relaxation models of Eqs. (1.1)–(1.7) to describe waves in turning-wind situations.

4. Constraints and basic analysis

In place of the constraints of section 2 for the $\mathcal{L}$ relaxation model, the following constraints were considered necessary for implementation and testing of the *fetch* relaxation model.

(v) In slanting fetch cases, Donelan et al. (1985) observed that the dominant wave is not in the direction of the wind but in the direction of the greatest energy input, which is at an angle to the wind. This motivates

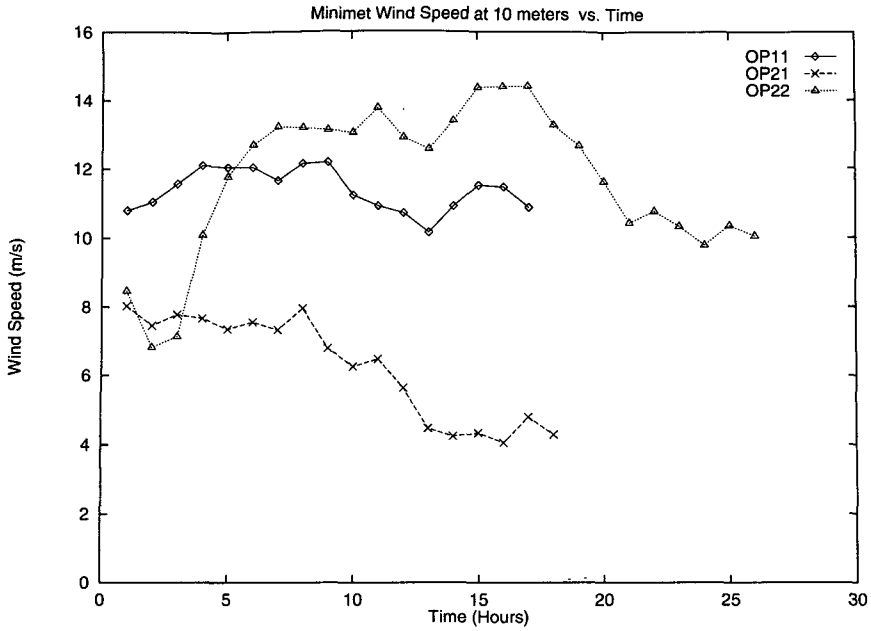

FIG. 4a. The wind speed as a function of time at the meteorological buoy during the observation periods OP11, OP21, and OP22.

the constraint that the wind direction θ_{10} must be within 60° to the left of orthogonal to the coastline: $\theta_{10} \in [-80°, -20°]$. Orthogonal to the shoreline is from −20°T, in degrees true. When $\theta_{10} \in [-80°, -20°]$, the dominant wave direction θ_p is always to the left of θ_{10}: $\theta_p < \theta_{10}$. In the domain $[-20°, 40°]$, the dominant wave direction θ_p is always to the right of the wind direction θ_{10}: $\theta_{10} < \theta_p$. Combining the data from both sectors gives complicated results, which appear noisy.

(vi) If the angle between θ_{10} and θ_p is too small, the response of the waves is noisy: $|\theta_{10} - \theta_p| > 5°$. Noise results from $1/\tan(\theta_{10} - \theta_p)$ in the denominator of Eq. (3.15). Van Vledder and Holthuijsen (1993) use the condition $90° > |\theta_{10} - \theta_p| > 10°$.

(vii) As the model assumes fetch-limited situations, the peak frequency must satisfy $|\Delta f_p| < 0.04$, where Δf_p is the change in f_p in succeeding time steps (1 hour). As time evolves, f_p must move to lower frequency and

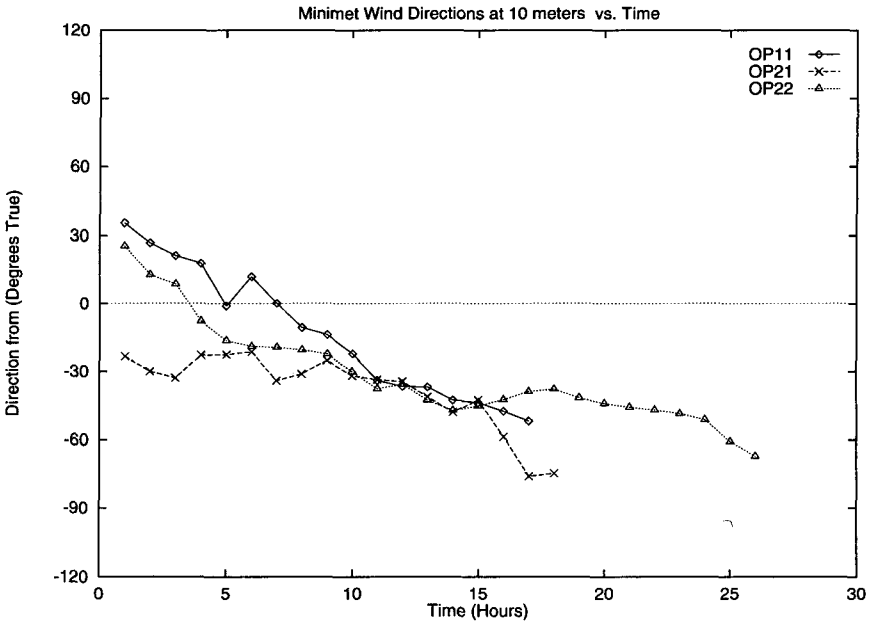

FIG. 4b. As in Fig. 4a but for wind directions θ_{10} as a function of time.

TABLE 2. Evaluation of Eqs. (5.5)–(5.6) neglecting $\mathcal{T}4$ and setting $\gamma = -3.35$. All data from observation periods OP11, OP21, and OP22 for the *fetch* relaxation model are presented. The right-hand side of (5.5) is represented as X, which is approximated as $1 + \mathcal{T}1 + \mathcal{T}2 + \mathcal{T}3$. The mean and mean square of X are denoted $\langle X \rangle$ and $\langle X^2 \rangle$. The number of observations is denoted n. The progressive effect of imposing the constraints are: (v), that $\theta_{10} \in [-80°, -20°]$; (vi), that $|\theta_p - \theta_{10}| > 5°$; (vii), that $|\Delta f_p| < 0.04$; and (viii), that $\mathcal{U}_{10} > 5$ m s^{-1}.

Constraint	Y_{min}	Y_{max}	$\langle Y \rangle$	$\langle Y^2 \rangle$	X_{min}	X_{max}	$\langle X \rangle$	$\langle X^2 \rangle$	$\mathcal{M}$	$\mathcal{B}$	n	$\mathcal{R}$
(v)	−21.1	176.8	3.29	335.4	−1.20	4.98	1.10	1.65	27.0	−26.4	119	0.75
(v) + (vi)	−21.1	176.8	3.34	338.2	−0.55	4.98	1.12	1.65	28.5	−28.5	118	0.78
(v) + (vi) + (vii)	−21.1	29.3	1.16	36.5	−0.55	2.31	1.03	1.21	15.0	−14.2	91	0.52
(v) + (vi) + (vii) + (viii)	−21.1	29.3	1.03	35.2	−0.55	2.31	1.03	1.20	15.8	−15.3	83	0.74

must not jump erratically as different parts of the spectrum gain momentary predominance. The threshold $|\Delta f_p| > 0.04$ assumes a modest rate of spectral growth as time progresses, following Resio and Perrie (1989).

(viii) The wind speed must satisfy $\mathcal{U}_{10} > 5$ m s^{-1} to avoid noise.

These constraints reduce episode (i) of section 2, which we now denote as OP11, to 17 hours from 1900 UTC 30 January to 1100 UTC 31 January. Whereas the *JONSWAP* relaxation model constraints (i)–(iv) lead to the highest correlations for a middle portion of episode (ii), the constraints for the *fetch* relaxation model (v)–(viii) select portions at the beginning and at the end of episode (ii). The divided episode (ii) is now denoted OP21: 18 hours from 0001 to 1800 UTC 14 February and OP22: 26 hours from 2200 UTC 15 February to 2300 UTC 16 February. These periods correspond to offshore wind situations. In fact, the wind direction θ_{10} is never more than ±60° from −20°T, which is the bearing of the directional wave buoy array orthogonal to the coastline. Figures 4a–b show the wind speed and direction as a function of time at the meteorological buoy during the three observation periods OP11, OP21, and OP22. The overall turning rates for these observation periods are 5.5, 3.0, and 3.7 degrees per hour, respectively. However, during segments within each observation period, turning rates were much higher.

Swell is always significant in the CASP wave spectra. Therefore, it is necessary to separate wind-generated sea spectra from swell spectra. Separation of swell from wind sea involves first determination of a critical frequency f_c. As described in Dobson et al. (1989) and Perrie and Toulany (1990), the separation frequency f_s is related to the critical frequency f_c, which is the lowest frequency in the wave spectra at which the phase speed is less than the wind speed component in the wave direction. The relation is

$$f_s = f_c - 0.03 \text{ Hz}, \tag{4.1}$$

where we have assumed that the wave spectrum has a forward face such that the distance to the half-power

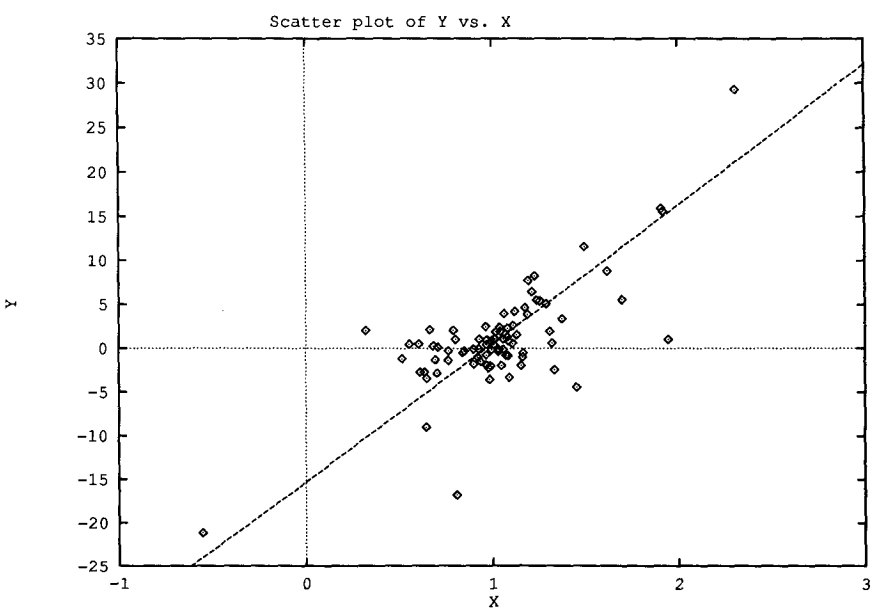

FIG. 5. The regression of X on Y for all buoys with the constraints (v)–(viii), as computed in Table 2.

TABLE 3. As in Table 2 and imposing all constraints (v)–(viii) at each buoy separately and at all buoys together.

	Y_{min}	Y_{max}	$\langle Y \rangle$	$\langle Y^2 \rangle$	X_{min}	X_{max}	$\langle X \rangle$	$\langle X^2 \rangle$	$\mathcal{M}$	$\mathcal{B}$	n	$\mathcal{R}$
WC31	−3.59	29.3	2.33	47.8	0.52	2.31	1.10	1.34	17.3	−16.7	25	0.75
WC32	−21.1	16.0	−0.12	40.3	−0.55	1.91	0.97	1.11	15.2	−14.8	32	0.70
WC33	−3.42	15.6	1.17	16.8	0.61	1.92	1.05	1.17	14.3	−13.8	26	0.82
All buoys	−21.1	29.3	1.03	35.2	−0.55	2.31	1.03	1.20	15.8	−15.3	83	0.74

point on the forward face is about 0.03 Hz, as shown by computations of the nonlinear energy transfer due to wave–wave interactions by Hasselmann and Hasselmann (1981).

5. Model verification

To simplify the discussion of the *fetch* relaxation model described by Eq. (3.15), we introduce the following set of labels:

$$\mathcal{J}1 = -\frac{1}{\tan\Delta\theta(f_p)}\left(\frac{1}{E_0(4+\gamma)}\frac{\partial E_0}{\partial\theta_{10}}\right) \tag{5.1}$$

$$\mathcal{J}2 = \frac{1}{\tan\Delta\theta(f_p)}\left(\frac{\gamma}{f_p(4+\gamma)}\frac{\partial f_p}{\partial\theta_{10}}\right) \tag{5.2}$$

$$\mathcal{J}3 = \frac{1}{\tan\Delta\theta(f_p)}\left(\frac{1}{\mathcal{U}}\frac{\partial\mathcal{U}}{\partial\theta_{10}}\right) \tag{5.3}$$

$$\mathcal{J}4 = \frac{1}{\tan\Delta\theta(f_p)}\left(\frac{1}{2C_d}\frac{\partial C_d}{\partial\theta_{10}}\right), \tag{5.4}$$

and we replace Eq. (3.15) by

$$\frac{\partial\theta_p}{\partial\theta_{10}} = 1 + \mathcal{J}1 + \mathcal{J}2 + \mathcal{J}3 + \mathcal{J}4. \tag{5.5}$$

Explicit measurements of $\mathcal{J}1$, $\mathcal{J}2$, and $\mathcal{J}3$ and the left side of Eq. (5.5) are provided in the CASP observations. Solving Eq. (5.5) for $\mathcal{J}4$, the rate of change of drag coefficient with a change in wind direction $\Delta\theta_{10}$ may be estimated. It is evident that verification of Eq. (3.15) and estimation of $\mathcal{J}4$ depends on estimates for γ. The most reliable estimates for γ reported by Perrie and Toulany (1990) are in the range from −3.35 to −3.44.

Writing $Y = \partial\theta_p/\partial\theta_{10}$ and $X \equiv 1 + \mathcal{J}1 + \mathcal{J}2 + \mathcal{J}3$, Eq. (5.5) may be written in the form

$$Y = X + \mathcal{J}4. \tag{5.6}$$

Because the drag coefficient was not measured during the CASP field program, we simply ignore $\mathcal{J}4$ and regress Y on X. Table 2 shows the effect of the constraints on all the data from OP11, OP21, and OP22, assuming that γ is −3.35. The regression analysis in Table 2 fits

$$Y = \mathcal{M}X + \mathcal{B} \tag{5.7}$$

and determines $\mathcal{M}$ and $\mathcal{B}$ empirically.

A perfect comparison between observations and the regression model given in Eq. (5.7), neglecting $\mathcal{J}4$ in Eq. (5.6), would imply a value of unity for $\mathcal{M}$. This is not achieved in Table 2. Because the number of observations is almost the same in the first and second rows of Table 2, constraint (vi) does not go much beyond what is achieved by constraint (v). Moreover, Y has quite large extremal values, denoted by Y_{min} and Y_{max}, compared to its mean $\langle Y \rangle$ and compared to the extremal values for X. Values for slopes $\mathcal{M}$ are large compared to unity. A quantitative change occurs, as recorded in the third row of Table 2, with the imposition of constraint (vii). Extremal values for X decrease slightly, and Y_{min} and Y_{max} decline dramatically. While $\langle X^2 \rangle$ has a slight decrease, $\langle Y^2 \rangle$ experiences a large decrease and $\mathcal{M}$ is smaller. However, the correlation coefficient $\mathcal{R}$ experiences a deterioration to 0.52. Constraint (vii) has significantly cleaned the data of outliers, as is evident from the reduced number of observations. This "cleaning of the data" is verified by the imposition of constraint (viii). The fourth row of Table 2 shows that values for $\mathcal{M}$, $\mathcal{B}$, and $\langle Y \rangle$ are maintained at the values established with constraint (vii). Moreover, $\mathcal{R}$ significantly improves. Figure 5 shows the regression of Y on X for all buoys when all constraints (v)–(viii) are imposed, corresponding to the fourth row of Table 2. The standard 95% confidence interval on the slope of the regression line is ±20%.

Table 3 presents the response of the three directional buoys separately, which compositely make up the last

TABLE 4. As in Table 3 with all the constraints (v)–(viii) assuming $\gamma = -3.44$. The Y statistics are as in Table 3.

	X_{min}	X_{max}	$\langle X \rangle$	$\langle X^2 \rangle$	$\mathcal{M}$	$\mathcal{B}$	n	$\mathcal{R}$
WC31	0.41	2.50	1.11	1.43	14.9	−14.3	25	0.75
WC32	−0.79	2.07	0.97	1.17	13.0	−12.7	32	0.70
WC33	0.53	2.05	1.05	1.21	12.2	−11.7	26	0.81
All buoys	−0.79	2.50	1.04	1.26	13.6	−13.1	83	0.74

TABLE 5. As in Table 4 but evaluating (5.5) and (5.6), neglecting $\mathcal{T}3$ and $\mathcal{T}4$. Constraints listed as (v)–(viii) are described in section 4. The right side of (5.5) is represented as X, which in this case is only $1 + \mathcal{T}1 + \mathcal{T}2$. Table 3 considers $X \equiv 1 + \mathcal{T}1 + \mathcal{T}2 + \mathcal{T}3$.

	Y_{min}	Y_{max}	X_{min}	X_{max}	$\langle Y \rangle$	$\langle Y^2 \rangle$	$\langle X \rangle$	$\langle X^2 \rangle$	$\mathcal{M}$	$\mathcal{B}$	n	$\mathcal{R}$
WC31	−3.59	29.3	0.19	2.43	2.33	47.9	1.12	1.45	14.4	−13.8	25	0.73
WC32	−21.1	16.0	−0.18	2.02	−0.12	40.3	1.00	1.18	14.7	−14.8	32	0.65
WC33	−3.42	15.6	0.57	1.90	1.17	16.8	1.05	1.20	12.9	−12.4	26	0.76
All buoys	−21.1	29.3	−0.18	2.43	1.03	35.2	1.05	1.27	14.4	−14.1	83	0.70

line of Table 2. That is, in Table 3, we have set $\gamma = -3.35$ and imposed all constraints (v)–(viii). Data from episodes OP11, OP21, and OP22 are presented, with X and Y as specified in Eqs. (5.5)–(5.7). Therefore, it is evident that the fourth row of Table 2 is the cumulative of the individual buoys shown in Table 3. The highest $\mathcal{R}$ (approximately 0.82) is obtained at the outermost wave buoy, WC33. Since this wave buoy is located at the same position as the meteorological buoy, this is not surprising. When γ is changed to −3.44 from −3.35, as presented in Table 4, values for $\mathcal{R}$ and $\mathcal{M}$ are slightly reduced compared to Table 3. Moreover, for each wave buoy and for the composite dataset, 65% to 76% of the correlation $\mathcal{R}$ of Y with $1 + \mathcal{J}1 + \mathcal{J}2 + \mathcal{J}3$ is accounted for simply by $1 + \mathcal{J}1 + \mathcal{J}2$, as reported in Table 5. When $\mathcal{J}3$ is added, which is the model X shown in Table 3, the correlations increase systematically by about 5%–6%. Attributing a further 5% (or better) to $\mathcal{J}4$ would put $\mathcal{R}$ in the range 75%–87% in Table 3.

That regression slopes are far from unity in Tables 2–4 implies that the straight line regression model given by Eq. (5.7) is inadequate. If it were valid to ignore the $\mathcal{J}4$ term, then the slope $\mathcal{M}$ in the regression relation would be near unity. Changing γ to force $\mathcal{M}$ to unity produces unphysical values for γ. Inclusion of the drag coefficient term $\mathcal{J}4$ in Eq. (5.4) is therefore necessary. In terms of root mean square values, Eq. (5.6) may be rewritten as

$$\sqrt{\langle \mathcal{J}4^2 \rangle} = \sqrt{\langle Y^2 \rangle - 2\langle YX \rangle + \langle X^2 \rangle}, \quad (5.8)$$

where $\langle\ \rangle$ denotes ensemble averages. An indication of $\sqrt{\langle \mathcal{J}4^2 \rangle}$ sensitivity with respect to γ is presented in Table 6. Table 6 considers γ values that more than span the range of all reported values for γ from field experiments. It is evident that $\sqrt{\langle \mathcal{J}4^2 \rangle}$ is largely insensitive to both γ and the wave age–dependent drag coefficient C_{d3} of Eq. (3.6). An estimate for $\sqrt{\langle \mathcal{J}4^2 \rangle}$ is

$$\sqrt{\langle \mathcal{J}4^2 \rangle} \approx 5.55, \quad (5.9)$$

averaging the first five rows of Table 6. As the corresponding mean $\langle \mathcal{J}4 \rangle \approx -0.01$, it follows that $\mathcal{J}4$ is noisy, computed as the residual $Y - X$. The 95% confidence level on $\langle \mathcal{J}4 \rangle$ is about -0.01 ± 1.

Direct field measurements of the drag coefficient implicit in $\mathcal{J}4$ are quite noisy, as shown in Smith et al. (1992) or Dobson et al. (1994). Therefore, it is expected that $\mathcal{J}4$ would be noisy. As discussed by Hoaglin et al. (1983) and Rousseeuw and Leroy (1987), the classical robust estimator for a variable contaminated with outliers is the median of $\mathcal{J}4$, denoted $\{\mathcal{J}4\}$. The median is the unique best estimator for very large samples from an arbitrarily contaminated symmetric unimodal distribution, rather than either the mean $\langle \mathcal{J}4 \rangle$ or the rms value $\sqrt{\langle \mathcal{J}4^2 \rangle}$. As given by their medians $\{\mathcal{J}4\}$, $\{X\}$, and $\{Y\}$, the best estimates for $\mathcal{J}4$, X, and Y are −0.538, 1.014, and 0.458, respectively. This demonstrates that while $\mathcal{J}4$ is an important complement to X, it does not dominate over X. Figure 6 presents the histograms for $\mathcal{J}4$, X, and Y. While outliers are present in the distributions of $\mathcal{J}4$ and Y, it is evident that most of values for $\mathcal{J}4$ and Y are in the neighborhood of their medians. As $\mathcal{J}4$ is inferred from the difference in X and Y, uncertainty in X or Y is reflected by uncertainty in $\mathcal{J}4$. Because most estimates for $\mathcal{J}4$ are near zero, contamination due to a few outliers, as displayed in Fig. 6, has a dominating influence on the

TABLE 6. Results for all buoys as a function of γ values with $n = 83$, $\langle Y \rangle = 1.03$, and $\langle Y^2 \rangle = 35.2$ as in the fourth row of Tables 3–4. In row three, the assumed drag coefficient is the wave age–dependent form C_{d3} from (3.6). In rows 5–6, the open-ocean long fetch C_{d2} of (3.5) is used.

Drag C_d	γ	X_{min}	X_{max}	$\langle X \rangle$	$\langle X^2 \rangle$	$\langle XY \rangle$	$\mathcal{M}$	$\mathcal{B}$	$\mathcal{R}$	$\sqrt{\langle \mathcal{T}4^2 \rangle}$
no C_d	−3.35	−0.55	2.31	1.03	1.20	2.66	15.8	−15.3	0.74	5.58
no C_d	−3.44	−0.79	2.50	1.04	1.26	2.93	13.6	−13.1	0.74	5.53
C_{d3}	−3.44	−0.75	2.50	1.04	1.25	2.82	14.0	−13.5	0.72	5.55
no C_d no $\mathcal{T}3$	−3.44	−0.18	2.43	1.05	1.27	2.74	14.4	−14.1	0.70	5.57
C_{d2}	−3.44	−0.86	2.50	1.04	1.27	2.95	13.5	−13.0	0.74	5.53
C_{d2}	−3.88	−7.30	7.41	1.20	5.81	10.1	2.80	−2.32	0.73	4.56

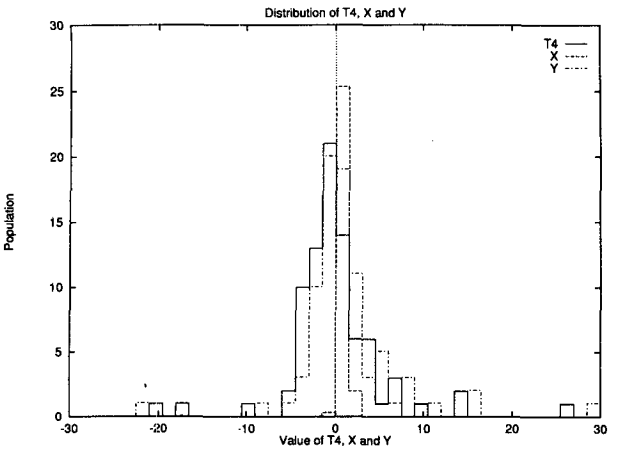

FIG. 6. Histograms for the $\mathcal{I}4$, X, and Y distributions. Because the X population is very narrow, it has been scaled by one-third.

mean and rms values for $\mathcal{I}4$ but does not bias the median of $\mathcal{I}4$.

6. Implications for the drag coefficient

From Eq. (5.4) and the estimate for the median $\{\mathcal{I}4\}$ presented in section 5, it follows that the best estimate for the variation in the drag coefficient is

$$\frac{\partial C_d}{\partial \theta_{10}} \approx -1.08\{\tan\Delta\theta(f_p)C_d\}, \qquad (6.1)$$

where $\Delta\theta(f_p) = (\theta_p - \theta_{10})$. Holding θ_p constant and integrating, we infer

$$C_d = C_{d0}\cos^{-1.08}\Delta\theta(f_p), \qquad (6.2)$$

where C_{d0} is the drag coefficient specified as C_{d1}, C_{d2}, or C_{d3} in section 3,

$$C_{d0} \approx C_{d0}\left(\frac{\mathcal{U}^2}{gz}, f_p^*\right). \qquad (6.3)$$

Here z is a reference height, and f_p^* the dimensionless peak frequency. A detailed formulation for C_{d0} in Eq. (6.3) follows from careful modeling of the wave boundary layer and its coupling to wind waves as given by Chalikov (1995), Chalikov and Belevich (1993), and Janssen (1989, 1991). It is of major importance that $\mathcal{I}4$ be negative. If $\mathcal{I}4$ were positive, our results are inconsistent with findings by Smith et al. (1992) that sea surface roughness Z_0 increases with new waves as compared to old waves.

When $\Delta\theta(f_p) = 60°$, the directional factor in Eq. (6.2) is $\cos^{-1.08}\Delta\theta(f_p) \approx 2$. Therefore, the significance of the 1.08 exponent is that large changes in the wind direction θ_{10}, relative to the dominant wave direction θ_p, have as large an effect on the drag coefficient C_d as young wave regimes, as measured by Smith et al. (1992) during HEXOS. However, the validity of Eq. (6.2) as determined from CASP data is somewhat limited. Very large shifts in wind direction were not present in our directional buoy data. As shown in Fig. 4b, the largest shift in wind direction, from one hour to the next, was about 20°. Large wind shifts of 60° in hour to hour records would give better estimates of $\mathcal{I}4$ if better estimates for Y were also obtained.

7. Concluding remarks

We have presented two models for the response of waves to forcing by turning winds: the standard $\mathcal{L}$ relaxation model given in Eq. (1.7) and a *fetch* relaxation model as derived in Eqs. (3.12)–(3.13). The $\mathcal{L}$ relaxation model is essentially the same as that of Hasselmann et al. (1980) and later researchers. It is distinctive in that it describes the response of waves to turning winds in terms of a timescale τ. Our analysis of CASP observations implies that τ obeys a quadratic variation with frequency f,

$$\tau \approx 10^4/[2\pi f(1.12f - 0.006)], \qquad (7.1)$$

where the correlation coefficient is 0.97 for this relation. The overall correlation $\mathcal{R}$ for the $\mathcal{L}$ coefficients within this relation is 0.55, comparable to results obtained by other researchers. It is notable that this correlation is not changed by *fetch* relaxation model constraints, such as (v), requiring that the wind direction be within the sector $[-80°, -20°]$.

By comparison, we have also derived and presented analysis for a *fetch* relaxation model displayed in Eqs. (3.12)–(3.13). Neglecting the normalized drag coefficient term $(2C_d)^{-1}\partial C_d/\partial t$, which was not measured in the CASP experiment, the overall correlation coefficient $\mathcal{R}$ is 0.74 for this relaxation model, as reported in Tables 2–4. Moreover, for the wave buoy WC33 immediately beside the meteorological buoy, $\mathcal{R}$ is about 0.82. In terms of the CASP data, this is the basis for the claim that the *fetch* relaxation model of Eq. (3.12) surpasses the $\mathcal{L}$ relaxation model of Eq. (1.7). This result is hardly surprising because, as written in its full form (3.12), the *fetch* relaxation model has six independent variables, θ_{10}, C_d, E_0, γ, f_p, and $\mathcal{U}$, whereas the $\mathcal{L}$ relaxation model of Eq. (1.7) depends on only two independent variables.

The *fetch* relaxation model indicates a role for the drag coefficient during turning winds, as shown by Eq. (6.2). For large wind shifts, such as 60° relative to a given mean wave direction θ_p, this relation implies a factor of ~2 for the amplication in the drag coefficient. When $\theta(f_p)$ is 75°, the amplication factor $\cos^{-1.08}\Delta\theta(f_p)$ is approximately 4. This is quite a large effect. The exponent, −1.08, is plausible because it results in a factor of 2–3, comparable to the increase in drag coefficients experienced for young waves as compared to old waves, from Smith et al. (1992).

Acknowledgments. The wave modeling program at BIO is funded by the Federal Panel on Energy Research and Development (Canada) under Project 62139.

REFERENCES

Allender, J. H., J. Albrecht, and G. Hamilton, 1983: Observations of directional relaxation of wind sea spectra. *J. Phys. Oceanogr.*, **13,** 1519–1525.

Chalikov, D., 1995: The parameterization of the wave boundary layer. *J. Phys. Oceanogr.*, **25,** 1333–1349.

——, and M. Yu. Belevich, 1993: One-dimensional theory of the wave boundary layer. *Bound.-Layer Meteor.*, **63,** 65–96.

Dobson, F., W. Perrie, and B. Toulany, 1989: On the deep-water fetch laws for wind-generated surface gravity waves. *Atmos.-Ocean,* **27**(1), 210–236.

——, S. D. Smith, and R. J. Anderson, 1994: Measuring the relationship between wind stress and sea state in the open ocean in the presence of swell. *Atmos.-Ocean,* **32**(1), 237–256.

Donelan, M. A., 1982: The dependence of the aerodynamic drag coefficient on wave parameters. *First Int. Conf. on Meteorological and Air/Sea Interaction in the Coastal Zone,* Le Hague, Amer. Meteor. Soc., 381–387.

——, J. Hamilton, and W. H. Hui, 1985: Directional spectra of wind-generated waves. *Philos. Trans. Roy. Soc. London,* **A315,** 509–562.

Gao, Q., and G. Komen, 1993: Directional response of ocean waves to changing wind directions. *J. Phys. Oceanogr.*, **23,** 1561–1566.

Günther, H., W. Rosenthal, and M. Dunkel, 1981: The response of surface gravity waves to changing wind direction. *J. Phys. Oceanogr.*, **10,** 718–728.

Hasselmann, D. E., M. Dunkel, and J. Ewing, 1980: Directional wave spectra observed during JONSWAP 1973. *J. Phys. Oceanogr.*, **10,** 1264–1280.

Hasselmann, K., T. P. Barnett, E. Bouws, H. Carlson, D. E. Cartwright, K. Enke, J. A. Ewing, H. Gienapp, D. E. Hasselmann, P. Kruseman, A. Meerburg, P. Müller, D. J. Olbers, K. Richter, W. Sell, and H. Walden, 1973: Measurements of wind-wave growth and swell decay during the Joint North Sea Wave Project (JONSWAP). *Dtsch. Hydrogr. Z.*, **12,** 95 pp.

Hasselmann, S., and K. Hasselmann, 1981: A symmetrical method of computing the nonlinear transfer in a gravity-wave spectrum. *Hamburger Geophys. Einzelschr.*, **A52,** 163 pp.

——, and ——, 1985: The wave model EXACT-NL. *The Sea Wave Modeling Project (SWAMP): Principle Results and Conclusions,* Plenum Press. 249–251.

Hoaglin, D. C., F. Mosteller, and J. W. Tukey, 1983: *Understanding Robust and Exploratory Data Analysis.* Wiley and Sons, 447 pp.

Holthuijsen, L. H., A. J. Kuik, and E. Mosselman, 1987: The response of wave directions to changing wind directions. *J. Phys. Oceanogr.*, **17,** 845–853.

Janssen, P. A. E. M., 1989: Wave-induced stress and the drag of air flow over sea waves. *J. Phys. Oceanogr.*, **19,** 745–754.

——, 1991: Quasi-linear theory of wind-wave generation applied to wave forecasting. *J. Phys. Oceanogr.*, **21,** 1631–1642.

——, G. J. Komen, and W. J. P. de Voogt, 1987: Friction velocity scaling in wind wave generation. *Bound.-Layer Meteor.*, **38,** 29–35.

Kahma, K. K., and C. J. Calkoen, 1992: Reconciling discrepancies in the observed growth of wind-generated waves. *J. Phys. Oceanogr.*, **22,** 1389–1405.

Longuet-Higgins, M. S., D. E. Cartwright, and N. D. Smith, 1963: Observations of the directional spectrum of sea waves using the motions of a floating buoy. *Ocean Wave Spectra,* Prentice-Hall, 111–136.

Masson, D., 1990: Observations of the response of sea waves to veering winds. *J. Phys. Oceanogr.*, **20,** 1876–1885.

Perrie, W., and B. J. Toulany, 1990: Fetch relations for wind-generated waves as a function of wind-stress scaling. *J. Phys. Oceanogr.*, **20,** 1666–1681.

Resio, D., and W. Perrie, 1989: Implications of an f^{-4} equilibrium range for wind-generated waves. *J. Phys. Oceanogr.*, **19,** 193–204.

Rousseeuw, P. J., and A. M. Leroy, 1987: *Robust Regression and Outlier Detection,* Wiley and Sons, 329 pp.

Smith, S. D., 1981: Coefficients for sea-surface wind stress and heat exchange. Bedford Institute of Oceanography Rep. BI-R-81-19, 31 pp.

——, 1988: Coefficients for sea surface wind stress, heat flux, and wind profiles as a function of wind speed and temperature. *J. Geophys. Res.*, **93,** 15 467–15 472.

——, R. J. Anderson, W. A. Oost, C. Kraan, N. Maat, J. DeCosmo, K. B. Katsaros, K. L. Davidson, K. Bumke, L. Hasse, and H. M. Chadwick, 1992: Sea surface wind stress and drag coefficients: The HEXOS results. *Bound.-Layer Meteor.*, **60,** 109–142.

Van Vledder, G. P., and L. H. Holthuijsen, 1993: The directional response of ocean waves to turning winds. *J. Phys. Oceanogr.*, **23,** 177–192.

Young, I. R., S. Hasselmann, and K. Hasselmann, 1987: Computations of the response of a wave spectrum to a sudden change in wind direction. *J. Phys. Oceanogr.*, **17,** 1317–1338.